A SMART WIRELESS INTEGRATED MODULE (SWIM) ON ORGANIC SUBSTRATES USING INKJET PRINTING TECHNOLOGY

A Thesis
Presented to
The Academic Faculty

by

Sebastian R. Palacios

In Partial Fulfillment
Of the Requirements for the Degree
Master of Science in Electrical and Computer Engineering in the
School of Electrical and Computer Engineering

Georgia Institute of Technology
May 2014

A SMART WIRELESS INTEGRATED MODULE (SWIM) ON ORGANIC SUBSTRATES USING INKJET PRINTING TECHNOLOGY

Approved by:

Dr. Emmanouil M. Tentzeris, Advisor
School of School of Electrical and Computer Engineering
Georgia Institute of Technology

Dr. Andrew F. Peterson
School of School of Electrical and Computer Engineering
Georgia Institute of Technology

Dr. Gregory Durgin
School of School of Electrical and Computer Engineering
Georgia Institute of Technology

Date Approved: 04/02/2014

ACKNOWLEDGEMENTS

I would like to thank my parents for their support. I would like to thank Professor Manos M. Tentzeris for his invaluable help and advice, as well as the committee members Professor Andrew Peterson and Professor Gregory Durgin for reviewing my work. Finally, I would like to thank Jill Auerbach and Julie Ridings from the Opportunity Research Scholars Program, Amin Rida, Sangkil Kim and Symeon Nikolaou.

TABLE OF CONTENTS

LIST OF TABLES

LIST OF FIGURES

LIST OF SYMBOLS AND ABBREVIATIONS

Radio Frequency	RF
SoP	System-on-package
SoC	System-on-chip
WSN	Wireless Sensor Network
LCP	Liquid Crystal Plummer
SWIM	Smart Wireless Integrated Module

SUMMARY

This thesis investigates inkjet printing of fully-integrated modules fabricated on organic substrates as a system-level solution for ultra-low-cost and eco-friendly mass production of wireless sensor modules. Prototypes are designed and implemented in both traditional FR-4 substrate and organic substrate. The prototype on organic substrate is referred to as a Smart Wireless Integrated Module (SWIM). Parallels are drawn between FR-4 manufacturing and inkjet printing technology, and recommendations are discussed to enable the potential of inkjet printing technology. Finally, this thesis presents novel applications of SWIM technology in the area of wearable and implantable electronics.

Chapter 1 serves as an introduction to inkjet printing technology on organic substrates, wireless sensor networks (WSNs), and the requirements for low-power consumption, low-cost, and eco-friendly technology.

Chapter 2 discusses the design of SWIM and its implementation using traditional manufacturing techniques on FR-4 substrate.

Chapter 3 presents a benchmark prototype of SWIM on paper substrate. Challenges in the manufacturing process are addressed, and solutions are proposed which suggest future areas of research in inkjet printing technology.

Chapter 4 presents novel applications of SWIM technology in the areas of implantable and wearable electronics.

Chapter 5 concludes the thesis by discussing the importance of this work in creating a bridge between current inkjet printing technology and its future.

CHAPTER 1

INTRODUCTION

Realizing the potential applications of WSNs requires sophisticated and efficient communication protocols, low-power consumption, and low-cost [1] [2]. Furthermore, sensors nodes should be small and deployed in large quantities [2], which emphasizes the need for low-cost and eco-friendly substrates suitable for mass production. Organic substrates use is one of the leading candidates for ultra-low-cost, small, and eco-friendly packaging of Radio Frequency (RF) devices [3]. Among some of the most recent developments, wireless System-on-Package (SoP) solutions have been presented by embedding chip components in organic substrates [4]; Ultra Wide Band (UWB) modules with antennas using organic substrates have been designed [5]; wireless transmitters using embedded passives on organic substrates operating at 27MHz have been realized [6]; and techniques for packaging of miniature biomedical sensors on organic substrates have been presented [7].

Organic substrate packaging brings benefits to engineers such as the advantage of using paper as a substrate for SoP solutions. Remarkably, organic substrates also enable inkjet printing, a fast prototyping and packaging technique, which is similar to the one found in residential inkjet printers, but that is being refined and optimized with more capable printers in laboratories so that it can be applied to circuits [1]. In terms of low-cost packaging, and the need for low-profile transceivers, inkjet printing on paper could be particularly appealing if three dimensional antennas could be replaced with planar, printed antennas, and if the manufacturing process can be as efficiently as it is currently performed on FR-4 manufacturing.

Paper is the cheapest and most widely used organic substrate in the world; additionally, paper is recyclable and made of renewable raw materials [8] which offers an

environmental friendly solution. Various papers have been published in the area of printed electronics, with inkjet printing characterization results offering promising RF characteristics [3]; consequently, sensor-enabled RFID tags on paper that communicate with WSNs have been already demonstrated with a data transmission frequency of 904.4 MHz [3][9]. The achieve the results by using inkjet-printing technology to transfer the circuit design pattern directly onto the substrate via silver nanoparticles without material waste or traditional printed circuit board (PCB) etching techniques, which in turn adds to the economical manufacturing value and eco-friendliness of this manufacturing technique[3].

This thesis presents the design of a fully-integrated wireless sensor module on organic substrates, referred to as Smart Wireless Integrated Module (SWIM). We first demonstrate a prototype which is realized and tested on FR-4 substrate with a commercial swivel antenna. Then, we migrate the FR-4 module to paper substrate with an entirely printed Planar Inverted-F Antenna (PIFA). The module is the first fully-integrated IEEE 802.14.4 and ZigBee compliant wireless sensor node on paper using inkjet printing technology. The term *smart* is used because when paper is used as an active material in sensors and actuators, it is called “smart paper” [8]. The thesis demonstrates the potential of inkjet printing technology, and focuses on uncovering and specifying the challenges that need to be addressed in order for inkjet printing to become a low-cost manufacturing technique suitable for mass production. Solutions to the challenges are proposed, as well as potential novel applications of SWIM technology in the area of wearable and implantable electronics.

CHAPTER 2

PROTOTYPE USING TRADITIONAL TECHNIQUES

2.1 System Level Design

SWIM is a System-on-Package (SoP) wireless sensor node solution operating at 2.4GHz with low-power consumption, in-system programing, and a printed PIFA antenna. As it can be noted in **Figure 1**, a System-on-Chip (SoC) solution was chosen to implement the module on an organic substrate. The CC2431 is a SoC tailored for IEEE 802.14.4 and ZigBee applications. IEEE 802.14.4 is a standard defined for WSNs focusing on low-power operation and applications which do not require high-rate communication. ZigBee is built upon IEEE 802.15.4 and is suited for sensor and control applications focusing on low-cost and low-power design of both star and mesh network topologies [10][11]. The SoC solution features an 8051 Microcontroller Unit (MCU) with a 128KB in-system programmable flash and 8 KB RAM, an eight-input 12-bit ADC, a radio based on the CC2420 RF transceiver, and an analog temperature sensor among other features.

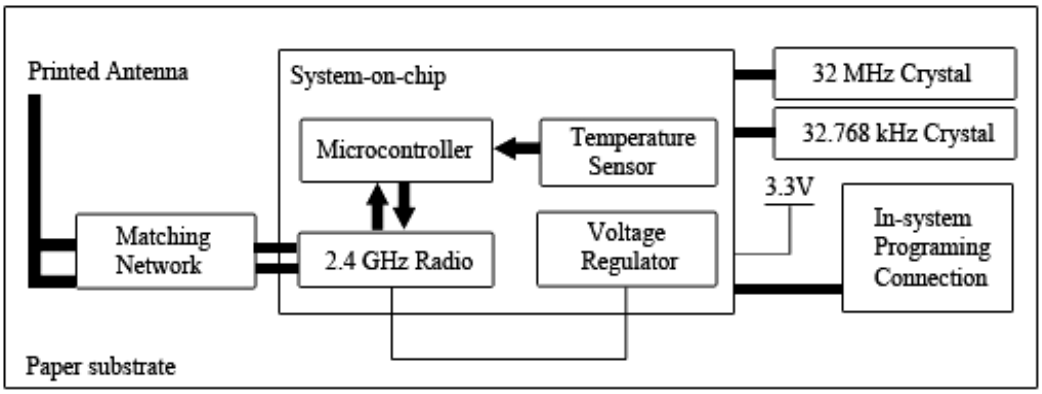

Figure 1. System level design of wireless sensor module on organic substrate.

The SoP is powered by an external 3.3V power supply, and the SoC voltage regulator is decoupled with external components to provide a regulated 1.8V power supply to the RF transceiver. The RF module uses an off-chip resistor as a precision passive component for current reference generation. The on-chip analog temperature sensor output is one of the inputs of the ADC multiplexer, so the MCU can be configured to read and broadcast the sensor readings. The SoC requires a 32 MHz crystal, and an optional 32.768 KHz crystal is added to improve power efficiency by allowing the SoC to switch clocks and enter various power consumption modes. An off-chip biasing resistor acts as a precision passive for current reference of the 32 MHz crystal oscillator. Programing and debugging of the chip is accomplished by a proprietary synchronous two-wire interface with a clock and a data line which also requires control of the SoC reset pin. Finally, a matching network described in [11] consisting of three inductors and one capacitor to match the differential impedance of the RF module to a 50Ω antenna is used. Additional components of the SoP include loading capacitors for the crystal oscillators and decoupling capacitors.

2.2 Module Integration

The realization of the SoP on FR-4 can be seen in Figure 2. The FR-4 prototype has all the components and traces on the top PCB layer, and the bottom layer is a solid copper pour acting as a ground plane. The top and bottom ground planes were coupled using via holes, which can be later removed in the paper module integration. Two surface mount or wire jumpers were needed to realize the module on one layer. The PCB design was realized using Altium Designer and the FR-4 board by a commercial PCB manufacturer.

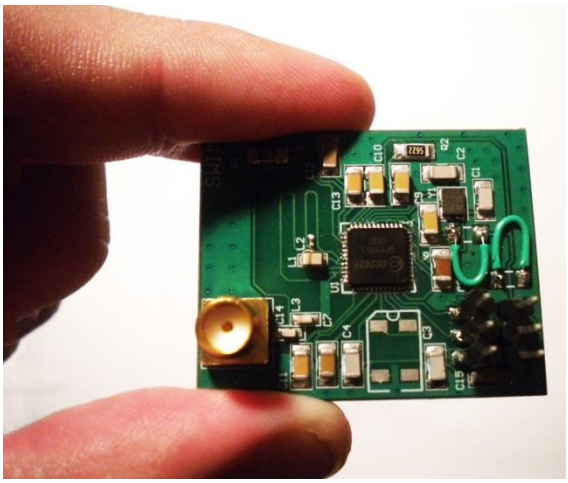

Figure 2. Designed wireless sensor module on FR-4 prototype.

Assembly was conducted manually using a microscope to place the components on their respective location over lead-based solder paste. A reflowing oven was used to attach the components to the board. As noted in Figure 3, a 50Ω Titanis 2.4 GHz Swivel antenna was used in the first prototype.

Figure 3. FR-4 prototype with commercial swivel antenna next to a 25 cents coin.

2.3 Module Testing

The SmartRF Studio software was used to evaluate and configure the FR-4 prototype. As seen in Figure 4, an evaluation wireless sensor module (CC2430EM) based on the CC2430 which also supports IEEE 802.14.4 and ZigBee was used to communicate wirelessly with the FR-4 prototype. The modules were positioned at 22cm of each other, each using a Titanis 2.4 GHz Swivel antenna. Both modules were set to transmit and receive 100 consecutive network packets with a random hexadecimal message on the 0x0B IEEE 802.14.4 channel with and transmit power of 0.6dBm. The FR-4 prototype correctly modulated, sent, and received the messages with an average RSSI measurement of -23.1dBm.

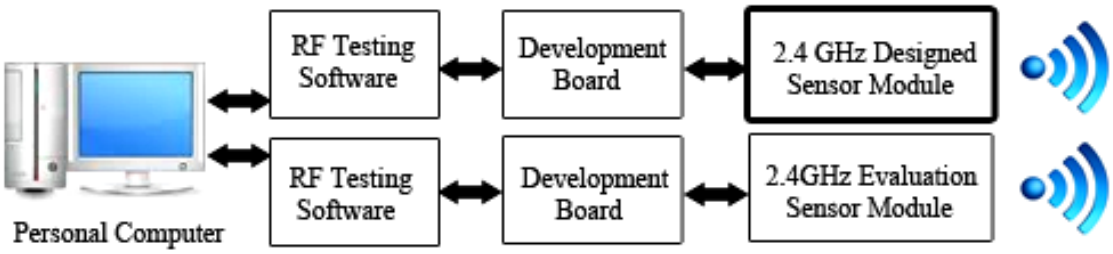

Figure 4. FR-4 and paper module prototype testing setup.

CHAPTER 3

BENCHMARK PROTOTYOPE ON ORGANIC SUBSTRATE

3.1 Module Design

Several approaches were proposed to accomplish a benchmark prototype on organic substrate. Figure 5 shows the PCB design of the inkjet-printed module in Altium Designer, and the antenna design in Ansoft's HFSS. This design has the same PCB design of the FR-4 module with the exception of the printed antenna, a slightly modified matching network, and the removal of via holes for which the SoC ground pad is now connected through the unused pins of the chip. The matching network described in [11] can be adjusted to work on paper. The passive components can remain the same, while varying the thickness and width of the transmission lines to accommodate for the dielectric properties of paper substrate described in [12]. An optional matching network that requires less variation is described in [13]. The proposed variation, obtained by using [14], is an estimated 50 mil width for the balun-to-antenna connection. The estimate was found using a 3.3 dielectric constant, 0.07 tangent loss, and 0.5mm substrate thickness [12]. The minimum trace width of the PCB is 0.254mm, and the minimum clearance between traces is 0.22 mm; this resolution has been already demonstrated in the laboratory, although the resolution depends on the ink material, the substrate, the curing processes as well as the voltage waveform used on the printer [9].

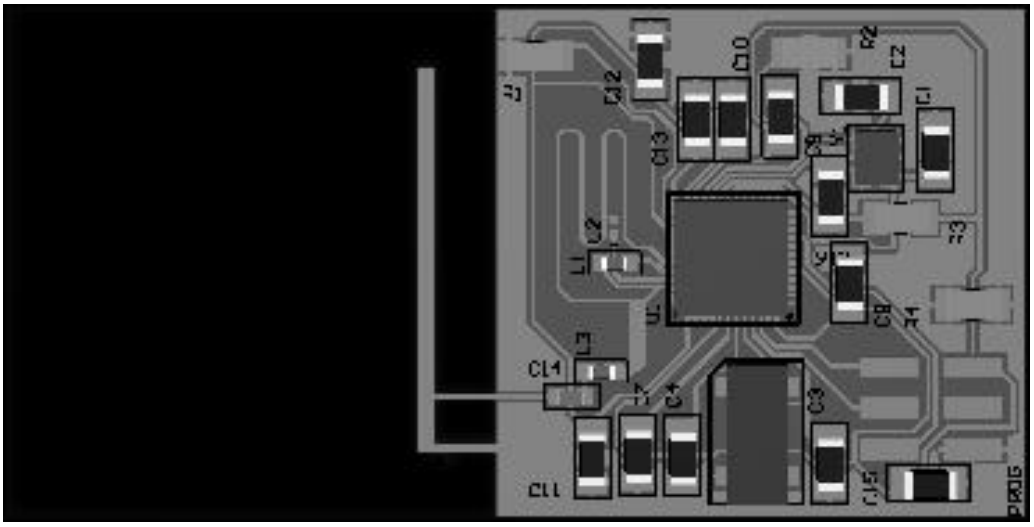

Figure 5. Paper substrate module design with printed antenna in Altium Designer.

3.2 PIFA Antennas

The first antenna design is a printed PIFA on 0.5mm thick paper. The antenna was designed in HFSS as seen in Figure 6. The S11 simulated recordings for the center frequency of the antenna were -16.4 dB, as shown in Figure 7, and the realized gain is 2.8dBi as noted in the radiation patters in Figure 8. The size of the feed is 0.254x3.6mm, the shorting pin is 3.6x19.24mm, the radiator is 23.5x1 mm, and the distance between the shorting pin and the radiator is 4 mm. The paper material used for the simulation has a 3.3 dielectric constant and 0.07 tangent loss as described in [12].

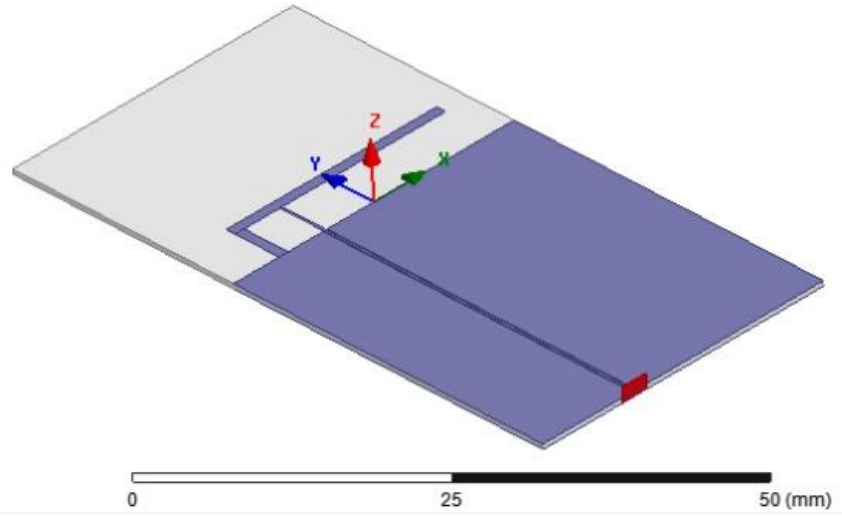

Figure 6. Paper substrate wireless sensor module antenna simulation in HFSS.

For the simulation, it is assumed that a matching network has been already realized, and a 50Ω wave port is used as exitation. The assembly technique suggested is described in [3], which replaces lead-based solder paste with conductive epoxy and does not require reflowing.

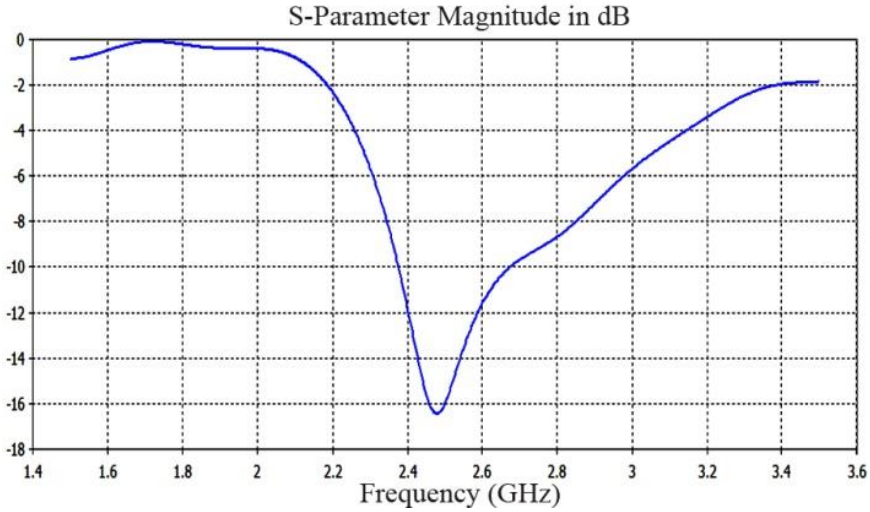

Figure 7. S11 parameters of printed antenna in HFSS.

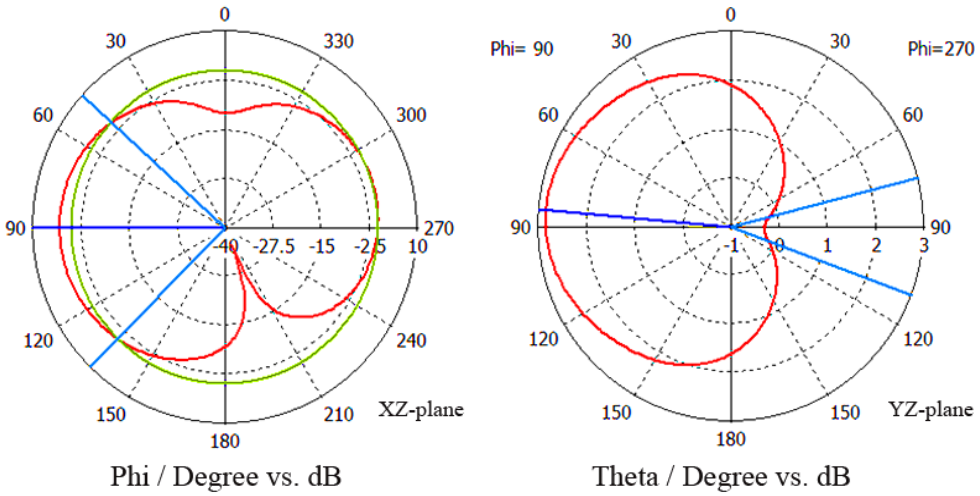

Figure 8. Radiation pattern of printed antenna in HFSS.

The secondary printed PIFA and module configuration was designed for SWIM, as shown in Figure 9. The design is generally analogous to the previous PIFA, but the traces have different dimensions, and the ground planes were extended. The Gerber file of the paper-based sensor module layout was created in Altium and then imported into HFSS for the design and integration of the planar PIFA.

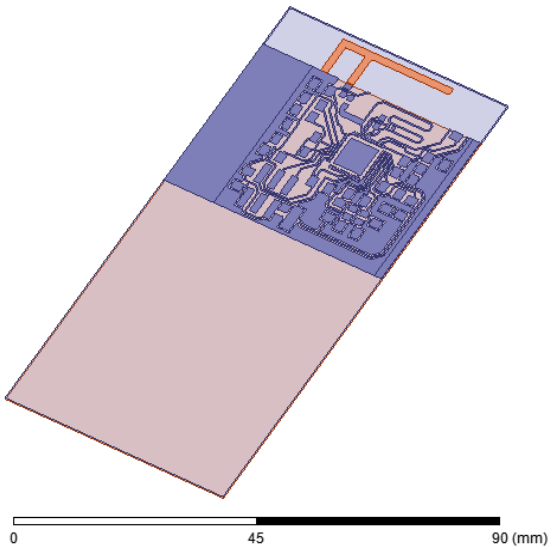

Figure 9. SWIM module on paper with second printed antenna in HFSS.

The second antenna was matched to 50 Ω and was designed using full wave simulation with the entire layout modeled as perfect electric conductor (PEC) in HFSS as seen in Figure 9 and Figure 10. The paper substrate used for the second module and antenna was 0.5 mm thick, with a 3.3 dielectric constant, and 0.07 tangent loss [9]. The dimensions of the module and antenna are described in detail in Table 1.

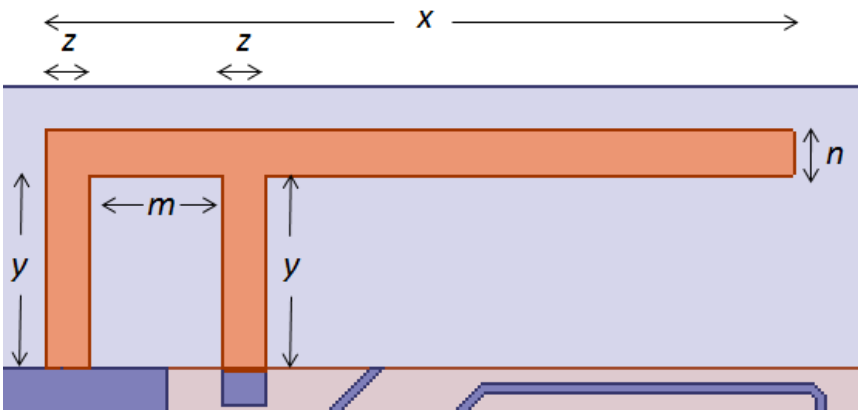

Figure 10. Second PIFA configuration on paper substrate.

Table 1. Second PIFA dimensions on paper substrate

Part	Dimension
z in Figure 10 in the short to ground, and n	1.48
y in Figure 10 in the antenna feed	6.42mm
x in Figure 10 in the radiating element	25mm
m in Figure 10 in between short and feed	4.44mm
Top ground plane in Figure 9	49.3mm x 34.3mm
Bottom ground plane in Figure 9	49.4mm x 89.32mm

One of the advantages of the co-design process of the antenna with the integrated PCB layout is the capability to modify and ultimately control numerous unique parameters. The optimization process indicated that the bottom ground plane had a significant role in the S11 characteristic that is shown in Figure 11. The reported S11 at 2.45 GHz is better than -18 dB, which is theoretically superior to the 3D swivel antenna in the FR-4 model. The ground plane is much larger in the paper-based solution; on paper the bottom ground is 49.4mm x 89.32mm and in FR-4 the ground size is 34.4 mm x 36.42mm.

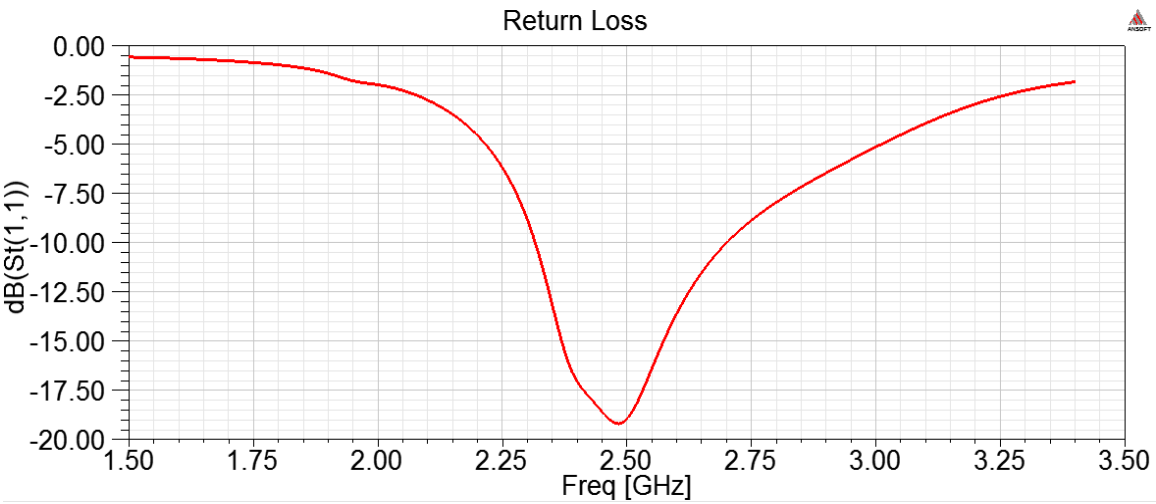

Figure 11. S11 characteristic of second printed PIFA antenna in HFSS.

The radiation patterns that can be seen in Figure 12 have a relatively omni-directional pattern in agreement with the reported patterns for the FR-4 sensor. The simulated results showed that the maximum return loss is -19dB, the efficiency is 78%, the back-to-front ratio is 2.2, and the peak realized gain is 2.9 dBi as it can be seen in in Figure 12.

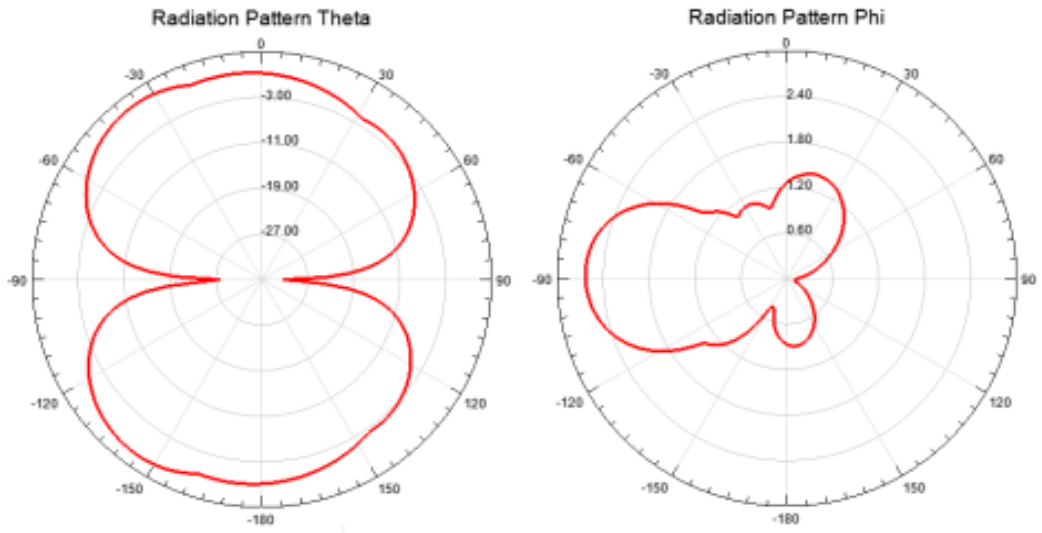

Figure 12. Radiation patterns of second PIFA peak realized gain in HFSS

These simulations suggest that the implementation of the layout of a commercial sensor on FR-4 with a 3D antenna can be inkjet-printed on paper substrate using a planar PIFA antenna. Despite the need for a larger ground plane, the reported planar antenna on paper in combination with the adjusted layout has better simulated return loss, gain, bandwidth and similar radiation efficiency as the swivel antenna used for the FR-4 module.

3.3 Folded Dipole Antennas

There are two main challenges with PIFA-based inkjet-printed wireless module design. The first challenge is that the matching network is relatively sensitive to shifting its impedance matching for small variations in the design, and because some of its traces are relatively thin and long, those traces may achieve high increases in impedance. The second challenge is that given that no standard technique exists to date to manufacture precise via holes, there is uncertainty as to how to connect the antenna with the required bottom ground layer, and there is lack of characterization of this type of connection at RF frequency in organic substrates.

One of best solutions is a folded dipole antenna matched to the RF module of the SoC. A folded dipole antenna can be printed on paper, it would not require a bottom ground plane, and it would only require one passive component for impedance matching. Figure 13 shows SWIM with a folded dipole antenna as described by [15]. This antenna is particularly suitable to this SoC as the two terminals of the folded dipole antenna serve as a DC connection between the two RF pins in the CC2431 SoC as it required for the RF module to transmit signals properly. There is only one capacitor required across the terminals of the antenna to match the antenna to the SoC2431 as shown in [15]. The connection from the center of the antenna to the SoC provides a virtual ground to the SoC, and an inductor is placed across this connection as a means to preventing any RF currents from leaking back to the SoC.

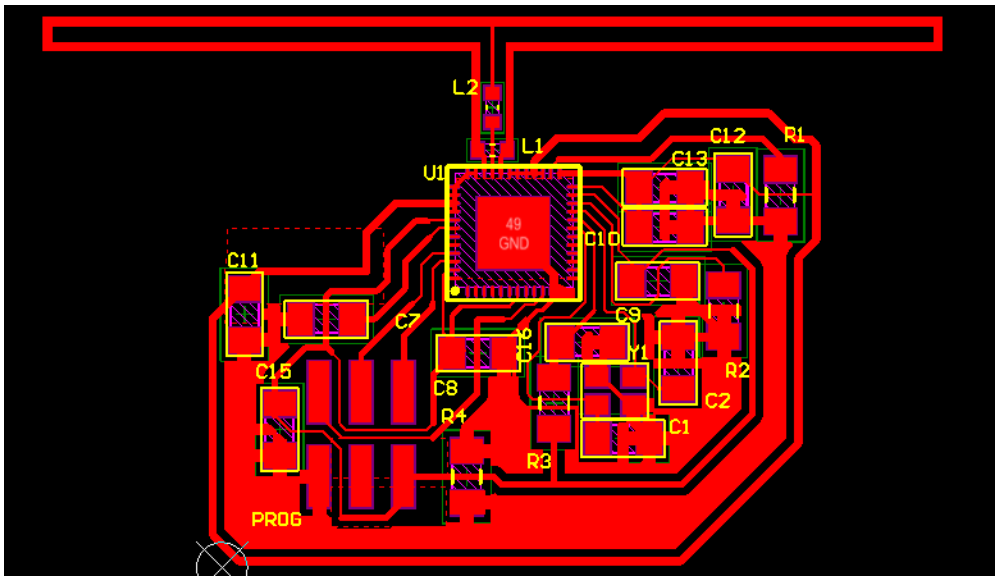

Figure 13. SWIM with folded dipole antenna.

Figure 2 shows the HFSS simulation of SWIM with the folded dipole antenna. The ground plane, antenna shape, and module geometry were recreated in HFSS. The

dielectric constant of the paper in the simulation is 3.3, the tangent loss is 0.07 and the paper thickness is 0.228 mm. This configuration is favorable for future assembly because this antenna does not require a bottom ground plane (i.e. no via holes) and has fewer components required for matching.

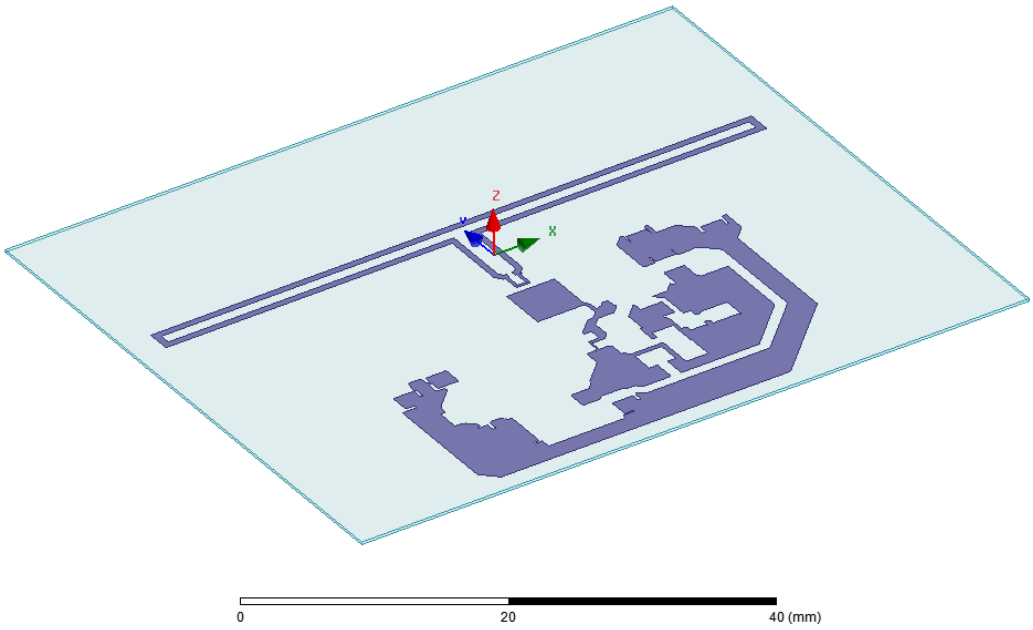

Figure 14. SWIM with folded dipole antenna in HFSS.

Figure 15 and Figure 16 show the results of the simulation, where the module had a resonant frequency at 2.45GHz with a peak of more than -20dB. The radiation pattern is clean and omni-directional with a 1.69dBi gain, and more than 90% radiation efficiency.

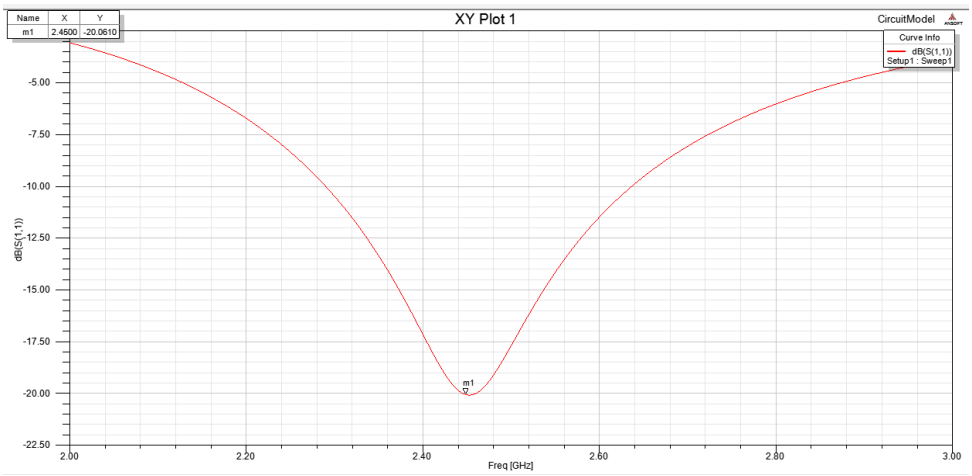

Figure 15. S11 parameters of SWIM with folded dipole antenna in HFSS.

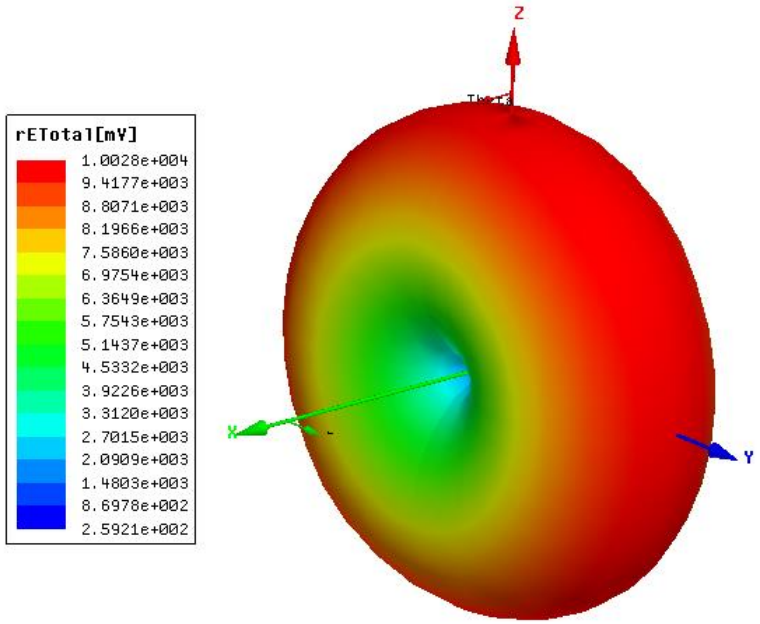

Figure 16. Radiation patter of SWIM with folded dipole antenna in HFSS.

The SWIM with the folded dipole antenna was inkjet printed on paper substrate with Gerber files produced from Altium designer. The assembly to realize the module shown in Figure 17 was conducted under a microscope using conductive epoxy to solder the components on paper, and the setup shown in Figure 4 was used to test the prototype.

Both modules were set to transmit and receive 100 consecutive network packets with a random hexadecimal message on the 0x0B IEEE 802.14.4 channel with and transmit power of 0.6dBm. The prototype correctly modulated, sent, and received the messages.

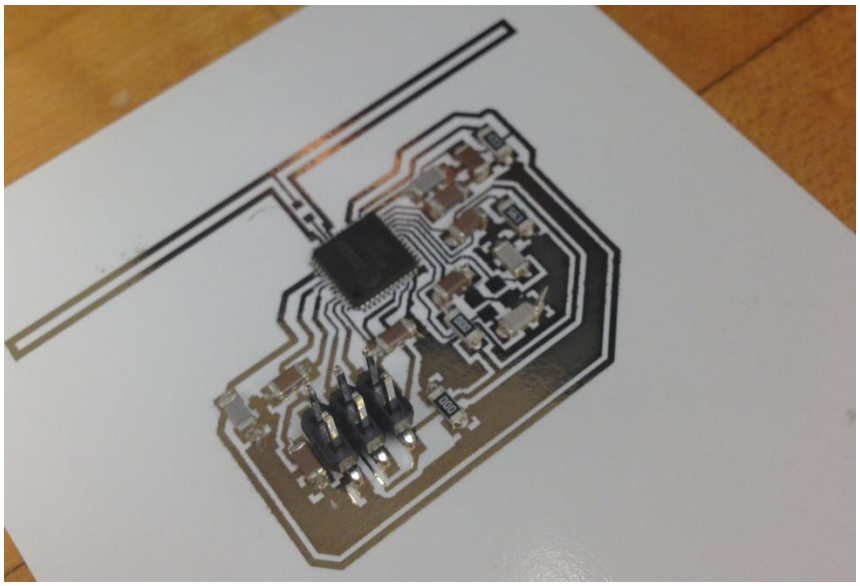

Figure 17. SWIM prototype on organic substrate using a folded dipole antenna.

3.4 Big challenges

Many papers had already demonstrated that planar antennas can be readily manufactured on paper using inkjet printing technology and printed traces have been shown to have relatively low impedance; therefore, it is not a surprise that a fully-integrated module can be built using inkjet printing technology. However, even though the design process is generally straight-forward, the assembly process is not as practical and well-defined. In this section we outline the main issues that need to be solved for inkjet printing to realize its potential for mass manufacturing of wireless modules.

3.4.1 Soldering Technique

In FR-4, as in chapter 2, solder paste is placed on the conductive pads where the surface mount components make the electric connection to the PCB. The solder paste is manufactured so as to attain a high surface tension during the reflow process. As the PCB modules are being reflowed, the surface tension of the solder paste minimizes the area of the melted solder paste forcing the solder paste onto the conductive pads. This leads to the reduction of short circuits during assembly, as well as self-alignment of the surface mount components.

On paper substrate, however, solder paste generally used for FR-4 manufacturing cannot be used because the temperature required to melt the solder paste damages the paper substrate. Therefore, the general approach that has been followed during the last few years is to use a cold soldering technique, such as using conductive epoxy. Manual assembly of the module becomes very difficult, as the conductive epoxy placement on the PCB does not allow error. In the other hand, traditional solder paste allows some room for error, as portions of the solder paste can be readily heated and removed. Soldering using conductive epoxy also needs to be precise since minimization of area and self-alignment of passive components do not occur. Furthermore, the conductive epoxy tends expand as it cures, increasing the probability of creating a short circuit. Finally, the conductive epoxy is relatively weak after curing as compared to solid bonds created by solder paste in FR-4. The high-precision requirements and issues associated with conductive epoxy also hinder automated processes of assembly.

3.4.2 Via Holes

Creating a fully-integrated wireless module will generally require at least two layers; generally for trace routing and ground planes. Since there is no standard way of incorporating via holes in paper substrates, the complexity of the designs are greatly

diminished. In the previous chapters, and in the benchmark prototype, we were able to demonstrate functionality by building the module completely in one layer. However, we had to route traces under the terminals of passive components, which is generally not a standard practice, and also increases the size of the module. Furthermore, as shown in the previous chapters, some antennas required a bottom ground place.

3.4.3 Long Term Durability

FR-4 generally has a long durability due to the strong bond between the conductive materials and the dielectric materials, and the silk screen. However, SWIM does not possess such a protective layer. Furthermore, the bond between the paper substrate and the conductive traces is generally weak, and small forces exerted on the module can crack the traces and damage the conductive layers. Additionally, as mentioned before, the conductive epoxy is relatively weak after curing, and a small force rip the components off the PCB.

3.5 Solutions

The first requirement to enable inkjet printing technology for mass manufacturing of wireless modules is utilizing a solder paste made with an alloy that melts before the organic substrate is damaged. This would allow reduction in the probability of a creating a short circuit, error correction, and self-alignment of components during the manufacturing process. The problem of via holes and silk screen protection are relatively more complex, as there are many options to attempt to solve this challenge. Laser perforations of the substrate combined with coating the paper with conductive material could be a potential solution to achieving via holes and multi-layer designs. The same is true for creating a protective layer for the module, where the module before assembly is covered with a layer or a protective material, such as a protective film. However, one of

the drawbacks of this approach is that adding extra steps to the process reduces the emphasis on inkjet printing technology and possibly increases the manufacturing cost. Ideally, a wireless module should be created using principally inkjet printing technology, and the wireless module should have the same characteristics as current wireless modules on FR-4. An ideal solution would be a printer that could print several materials so that the protective layers, for example, could be printed during an integrated process along with the conductive traces. Taking it a step further would be having an inkjet printer that can print conductive material through the laser-perforated holes of the paper. This would require a high-resolution and stability, as well as the software tools to print with multilateral components in a single integrated process. One step further, would be to print the organic substrate, and embedding conductive layers in the process, as well as the via holes.

Recently, new developments in 3D printing have led to the ability of printing objects of various materials. Currently, however, only a handful of printers can print with both high-resolution and multi-material objects [16]. Additionally, those printers have a prohibitive cost to the average user. For example, one of the printers that can print with two materials with high resolution is the Object Connex series, with a price of approximately $250,000. One of the possible enabling technologies for inkjet printing technology is a new type of printers being developed in the Computational Fabrication Group at the Massachusetts Institute of Technology for under $10,000. This printer has been shown to achieve high resolution during multi-material printing. The printer uses inkjet printing to produce 3D objects from a computer model. The same computer models used in Altium designer and HFSS could be used to guide the 3D inkjet printing process, where the 3D printer would ideally print the substrate along with the conductive traces. Further, multi-material printing could enable the printing of via holes during a fully-integrated printing process, where the whole module is printed together. For a two-layer module, for example, the printer can lay down some supportive material, and start

printing the bottom protective layers, and the conductive traces of the bottom layer on the protective layer. It then can print the substrate the embedding via holes in the substrate, or print the substrate with openings, and then fill them with conductive material to create the via holes. Then the top conductive traces would be printed, and a protective layer right after that. Additionally, since 3D printing allows multi-color printing as well, the components could be annotated as it is done on FR-4 manufacturing. The module would be then ready for applying solder paste, mounting the components and reflow. In the future, all of the passive components would be also printed using inkjet printing. Therefore, the assembly of a 3D module will only require mounting the most complex components such as the microcontroller.

CHAPTER 4

APPLICATIONS

4.1 Implantable Modules

As discussed in previous chapters, research has been conducted in creating low cost and durable wireless modules in biomedical applications using inkjet printing technology. These wireless modules have been made as wearable sensors, but recent projects have created sensors that can be implanted into human and other animal tissue [17]. Implantable antennas have traditionally been plagued by interference from dispersive tissue resulting in signal loss when placed on or near the tissue [18]. Placing the antenna in a dielectric has been demonstrated as decreasing this effect [19]. Researchers have also worked to reduce signal loss by creating printed electromagnetic band-gap structure (EBGs) arrays that filter signals when placed on or near the body, but these systems have only been demonstrated while having a large surface area [20][21].

Many of these wearable and implantable wireless modules utilize planar inverted-F antennas (PIFAs) due to their high front-to-back ratio and the relatively low impact of dispersive tissue on signal transmission when compared to other types of antennas [22]. However, PIFAs generally have very narrow bandwidths causing even minimal interaction between the tissue and the antenna to impact the system greatly. Researchers have been able to increase the bandwidth of PIFAs by etching away an area of the ground plane [23].

We describe the possibility of manufacturing low cost wearable and implantable modules with bandwidth-enhanced PIFAs in the low GHz frequencies using inkjet-printing technology. Previous research has shown that the optimal operating frequency of

these implantable antennas has been shown to be in the low GHz range [24]. Our module will incorporate an antenna operating at 1.86 GHz, a frequency which researchers have used demonstrating the lowest absorption loss in certain antennas while successfully transmitting power and data [25].

4.1.1 Antenna Design and Sensor Module

The wireless module has a standard architecture consisting of an embedded microprocessor, a matching network, a transceiver, an antenna, and a battery as shown in Figure 18.

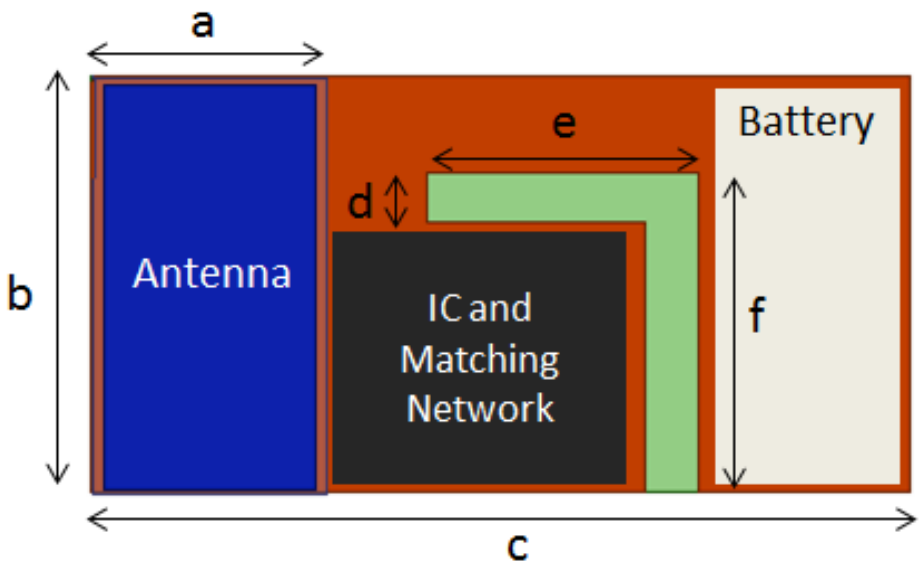

Figure 18. Implantable wireless module layout and dimensions.

The antenna lays on top of a ground plane as shown in Figure 19. The antenna consists of a stack of non-conductive layers with a 3.4 dielectric constant in the HFSS

simulations. Common substrates used in inkjet printing technology such as paper or Kapton have dielectric constants of 3.3 [12] and 3.4 respectively. The top layer of the antenna must be conductive and connected to the ground plane through the shorting pin(s) near the end of the antenna. Additionally, the top layer must be connected to the matching network through a separate pin, located 2mm away from the shorting pin(s). The shorting pins are 400 μm in diameter in the simulations.

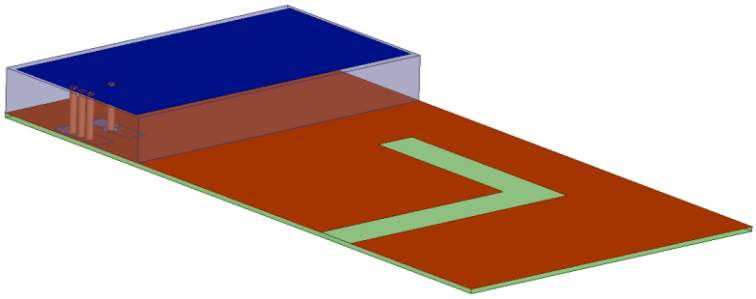

Figure 19. PIFA antenna in HFSS with ground slot.

The total size of the module is 19.5mm by 39mm, and the antenna is 11mm by 19.5mm. Parametric HFSS simulations determined that the slot geometry shown in Figure 19 can be used to enhance the antenna's bandwidth; its dimensions and the dimensions of the module are found in Table 2.

Table 2. Antenna configuration dimensions

Part	Dimension
a in Figure 18 is the width of the antenna	11mm
b in Figure 18 is the length of the antenna	19.5mm
c in Figure 18 is the length of the module	39mm
d in Figure 18 is the width of the ground slot	2.3mm
e in Figure 18 is part of the ground slot	13mm
f in Figure 18 is part of the ground slot	15mm
Antenna height, substrate thickness	2.5mm, 250μm

4.1.2 Results

The return loss of the wireless module can be seen in Figure 20. The antenna's resonant frequency is 1.86GHz and it has been bandwidth-enhanced. This frequency has not been tested using PIFAs, so we only demonstrate that inkjet-printing technology can possibly be used to manufacture this type of antenna and modules in that frequency range.

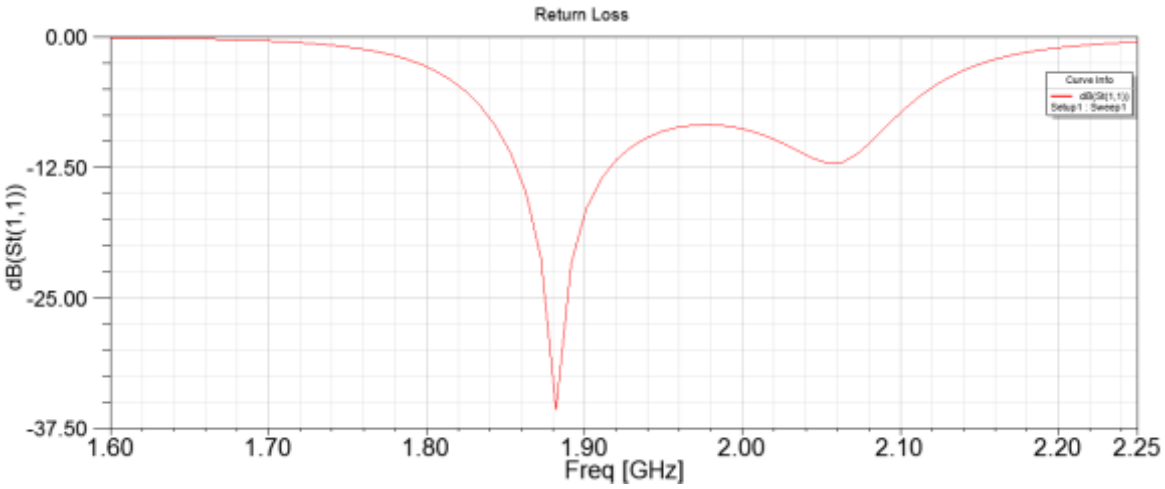

Figure 20. Implantable wireless module S11 parameters.

Figure 21 shows the radiation pattern of the module with a radiation efficiency of more than 90%, and 1.5dBi realized gain. This presents the possibility of manufacturing low cost wearable and implantable modules with PIFA antennas in the low GHz frequencies using inkjet-printing technology. The antenna has been bandwidth-enhanced by loading it with a ground slot.

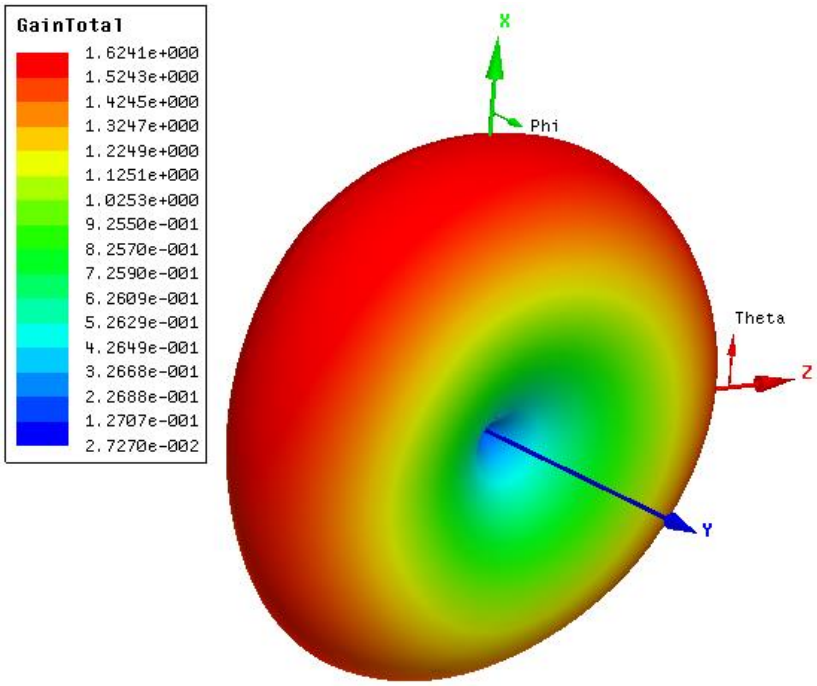

Figure 21. Implantable wireless module radiation pattern.

4.2 Wearable modules and 3D inkjet-printed antennas

In this section we explore a wearable module similar to the one presented in section 4.2, but with the concept of a 3D printed antenna at a more commonly used frequency of 2.45GHz. This module has an antenna that can be 3D printed, which consists of a polymer with a specific dielectric constant, a rectangular shape, and a printed conductive layer on top. This configuration corresponds to a PIFA antenna, and therefore it needs a shorting pin and a feed from the RF module. PIFAs have been used in mobile applications for decades, but they did not start to be studied for various wearable applications until the last decade where they have shown small losses associated with the presence of the body in the near-field of the antenna [26].

4.2.1 Antenna and Model

The antenna is just a rectangle with total size of 20.5x3.6x3.3mm (length, width, and height) and lies on a ground plane. The shorting and feed pins are located 1.3mm from the antenna's edge, and 1.6mm from each other. All the pins were modeled in HFSS with a 0.4mm diameter. The antenna's printed conductive layer is 17.7x3.3mm.

The model consists of a top and a bottom ground plane, separated by a 62 mil substrate with a 4.4 dielectric constant, and 0.02 dielectric loss tangent. The antenna was placed 3mm apart from the substrate's edge. A similar antenna with FR-4 substrate and different dimensions 18x4x2.4mm (length, width, and height) is described in patent application [27], and exhibits a 2.45GHz resonant frequency but it is not studied for wearable applications or 3D inkjet-printing.

The wearable module model in HFSS is excited by a 50Ω wave port, connected by a 50 Ω coaxial line to the antenna's feed pin. The ground planes and conductive printed layer were modeled as perfect conductors with perfect E boundary conditions, and the pins were modeled as Perfect Electric Conductors (PEC). A radiation boundary was used with free space between the module and the model's boundary of more than λ/4, where λ is the wavelength in free-space. The solution frequency used was 2.45GHz with a maximum delta S 0.02, lambda refinement with a lambda target of 0.3333, the iterative solver enabled with a relative residual 0.0001, and a maximum delta Zo of 2%. All the simulations were conducted in a computer with a 6GB RAM memory and an Intel Core i7 CPU.

4.2.2 Radio Frequency parameters

A frequency sweep from 1.5GHz to 3.4GHz with a 200 linear count was conducted. There are several things that contribute to the impedance of the antenna as well as its performance including the size of the ground plane, the location of the antenna on the ground plane, and the distance between the antenna's shorting and feed pins [28]. As seen in the S11 parameters in Figure 22, the antenna has a 2.45GHz resonant frequency and a peak return loss of 24.8dB, which indicates impedance close to 50Ω and 0.33% impedance mismatch.

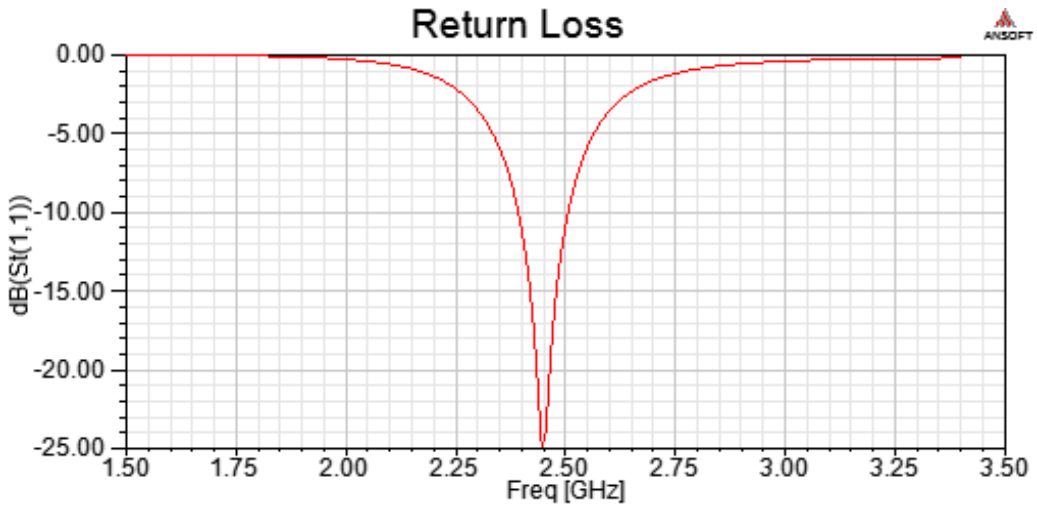

Figure 22. Wireless wearable module's free-space return loss.

The analysis produced a 2.62dBi peak realized gain as seen in Figure 9, radiation efficiency of 80%, and a 2.64 front-to-back ratio which indicates that the power is mostly radiated towards the front of the module. The ground plane size is a factor in the peak

realized gain, as the ground plane in this type of antenna directs the radiated power of the antenna towards the front [29], which also influences the front-to-back ratio.

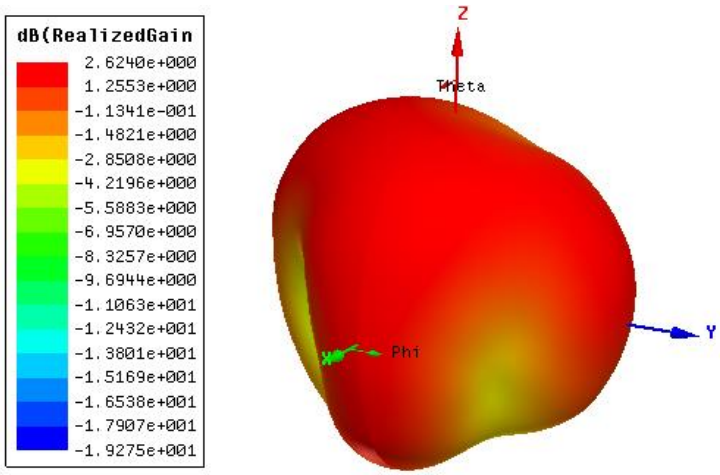

Figure 23. Wireless wearable module's free-space radiation pattern.

4.2.3 Specific Absorption Rate (SAR)

An optimal body-worn RF performance is necessary for reliable data communication, especially as the distance between transceivers increases. This section describes the body-worn RF performance of the wireless module. A model recommended by the FCC to conduct SAR investigations is used to calculate the SAR of the wireless module in HFSS. Finally, a model with the dielectric properties of human tissue is used to study the body-worn RF performance of the wireless module.

The transfer of energy from electromagnetic fields in any material is described by the SAR. This measure is the time rate at which energy is absorbed by a specific medium when exposed to a radio frequency, normalized to the mass of the material exposed. The

SAR is the most reliable indicator of the potential biological effects of electromagnetic radiation inside the human body [30]. This measurement has been emphasized in the recent wake of the possible carcinogenic hazard of cellphones [31].

Portable transmitters carried by users typically operate with an output power of less than 100mW; however, even at low power levels, relatively high field strengths could be expected near the antenna [32]. The FCC defines the applicable SAR limit for a transmitting device in direct contact with the skin or within 20cm of a human body at 1.6W/Kg, averaged over 1g of tissue [32]. The FCC describes in [32] the guidelines for evaluating compliance with human exposure to RF electromagnetic fields, and [33] describes a computational method in HFSS to calculate the SAR. The calculation satisfies the relationship between the RMS electric field, tissue conductivity, and mass density [32].

The FCC recommends the use of a flat phantom model to calculate body-worn SAR, with a 52.7 dielectric constant, 1.95 S/m conductivity, and 1000Kg/m^3 at 2.45GHz. The length and width of the phantom should be at least twice the corresponding dimensions of the test device, including its antenna. A 2.0 ± 0.2 mm thick shell should surround the flat phantom, and should be made of a low-loss material with a dielectric constant of less than 5.0 and a loss tangent less than 0.05 [32].

A CAD model of a 1.74cm tall human was imported into HFSS, and a flat phantom was created from a section of its torso as seen in Figure 24. The phantom's dimensions are 30.6x30.1x23.2cm (height, length, width), with length and width as close to the torso dimensions as possible, and height more than twice the dimensions of the

wireless module. The phantom has a 2mm thick shell recommended by the FCC, with a dielectric constant of 1, and zero loss tangent to account for the maximum possible SAR.

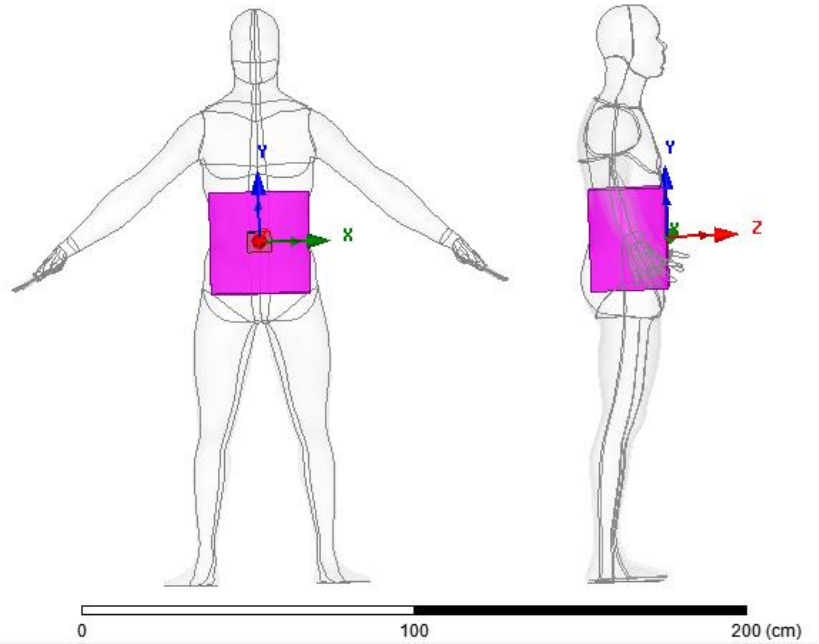

Figure 24. Body phantom based on FCC guidelines model in HFSS.

The wireless module was located as shown in Figure 24, lying on the outer face of the 2mm shell. Using the recommended dielectric properties and mass density of human tissue, the SAR for the entire phantom was obtained at 2.45GHz as shown in Figure 25. By definition, the SAR is averaged over 1g of tissue; therefore, this step is used to locate the place of maximum absorption in the phantom and place a 1g averaging volume as described in [33]. The HFSS field calculator was used to find the location of maximum SAR and place the 1g of tissue volume with the same dielectric properties and mass density of the larger phantom. The command in the field calculator is *MaxPos (Volume*

(Tissue), LocalSAR), where the only variable is *Tissue* and refers to the name of the volume over which the maximum SAR is being located [33].

Finally, the SAR averaged over 1g of tissue at the location of maximum SAR is 0.329W/Kg. The calculated result is normalized to 1W of output power [34], so the result needs to be adapted to the output power of the wireless module radio and also the duty cycle must be taken into account. $SAR = (SAR_{HFSS})(Duty\ Cycle)(P_{OUT})$ describes the relationship between the transmission duty cycle, output power, and HFSS [33], where SAR_{HFSS} is the 1W normalized calculated SAR, *Duty Cycle* is the transmission duty cycle, and P_{OUT} is the output power of the radio.

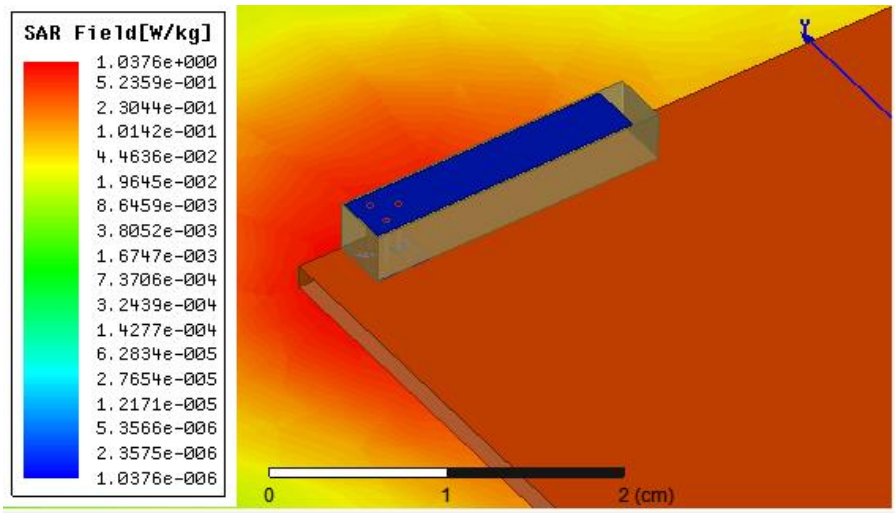

Figure 25. SAR plot in HFSS normalized to 1W of radio output power.

The IEEE 802.15.4 standard has the ability to provide duty cycles from 100% (generally not used) to 0.1% [34], and the wireless module radio has a 3 dBm or 2mW

output power. Using the two limiting values 2mW and 100% duty cycle, the wireless module has a SAR of 0.658mW/Kg.

4.2.4 Return loss and detuning

The same model used for the SAR calculation is used for modeling the wireless module body-worn parameters, but this time including the dielectric loss tangent of human muscular tissue at 2.45GHz [35]. There is an important consideration when modeling the return loss of the wireless module, and it is the fact that dielectric properties of human tissue are different at every frequency. The dielectric constant of muscular tissue was obtained from [35], and plotted in Figure 26.

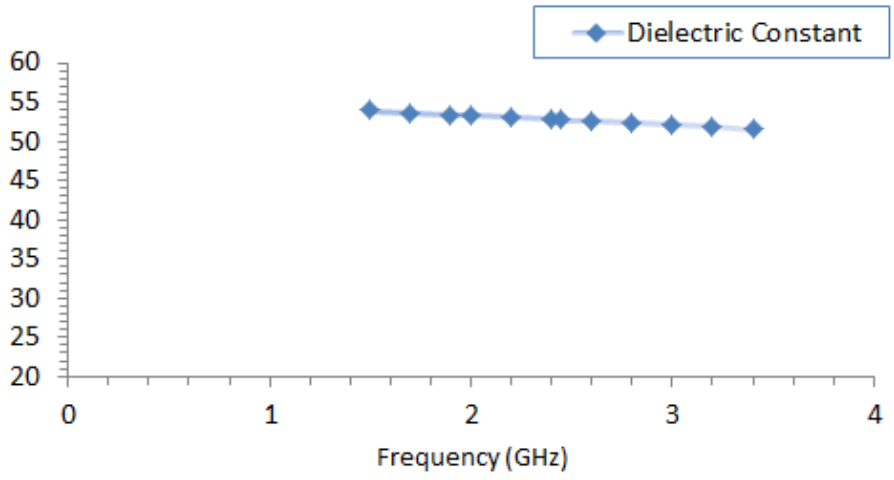

Figure 26. Dielectric constant of muscular human tissue for various frequencies.

As it can be seen in Figure 26, the dielectric constant remains reasonably constant over the range of frequencies used in the HFSS model. The loss tangent also varies with

frequency, so it was also obtained from [35], and plotted in Figure 27 over the range of frequencies used in the HFSS model. Although the loss tangent varies for different frequencies, it remains relatively constant over the range of frequencies analyzed.

Assuming the dielectric constant and loss tangent are the same for the range of frequencies from 1.5GHz to 3.4GHz, and the fact that the *phantom's height >> antenna*, the RF performance of the wireless module was simulated in HFSS using the same analysis set-up described for the SAR calculation and a loss tangent of 0.24194 [35].

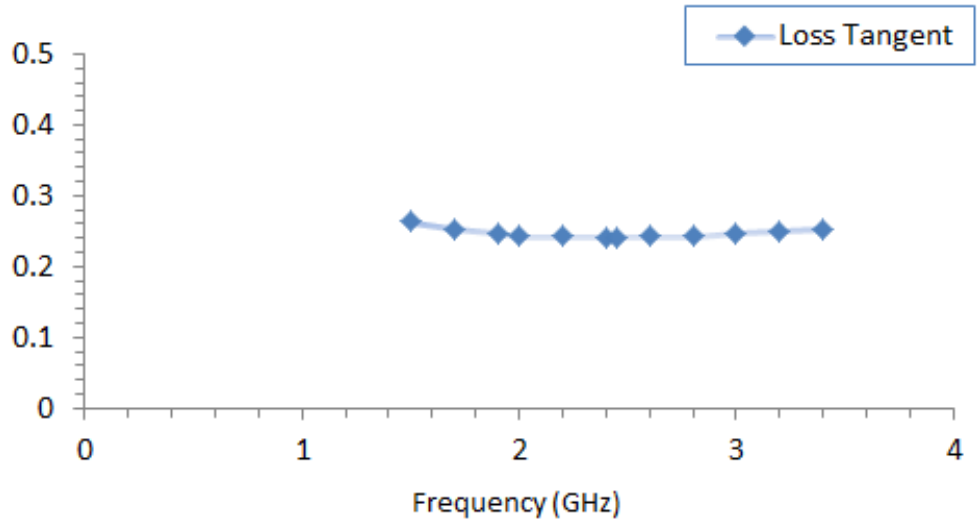

Figure 27. Dielectric loss tangent of muscular human tissue for various frequencies.

The results of the simulation can be seen in Figure 28, where only a small shift in the S11 parameters is observed and the resonant frequency is still significantly below -10dB line.

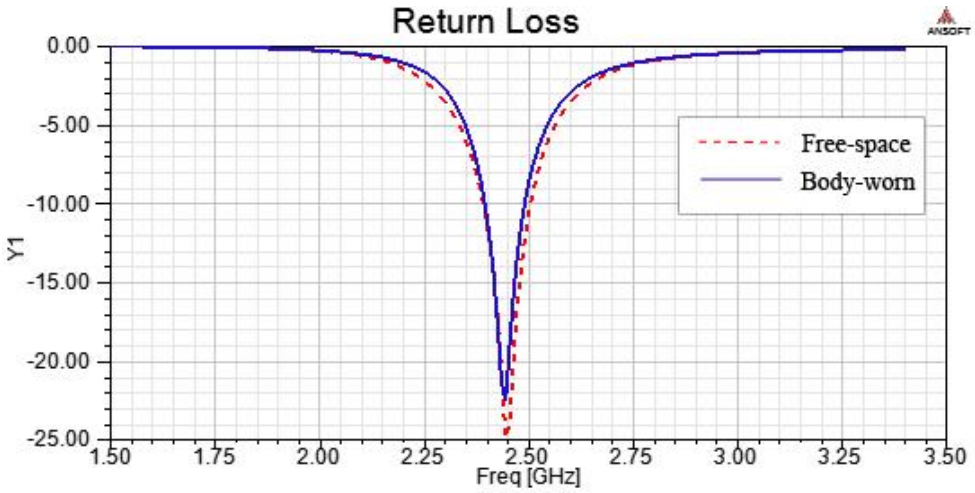

Figure 28. Antenna detuning in presence of tissue in the near-field.

The radiation patterns of the wireless module changed due to the presence of the human body in the antenna's near-field, as it can be seen in Figure 29 and Figure 30.

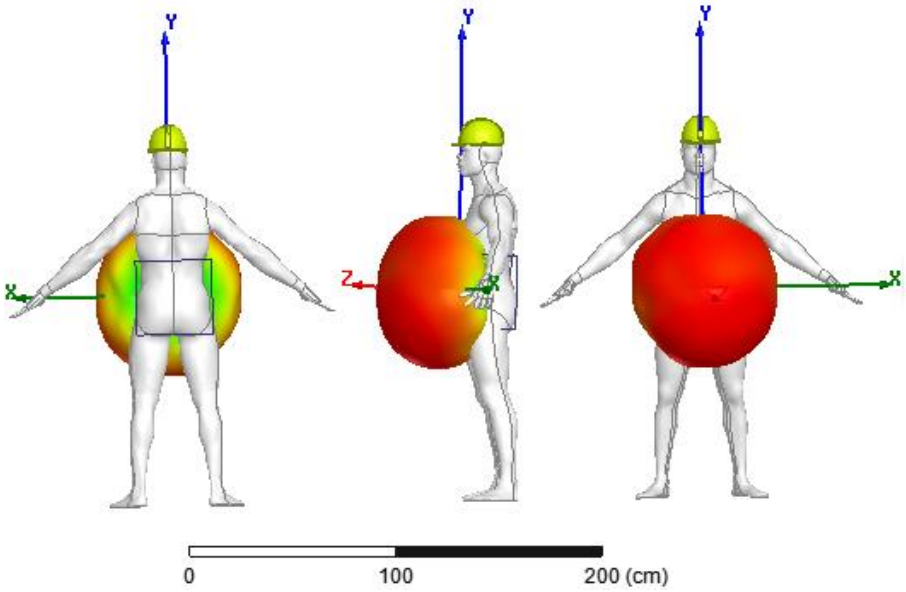

Figure 29. Radiation pattern of module on body phantom based on FCC guidelines.

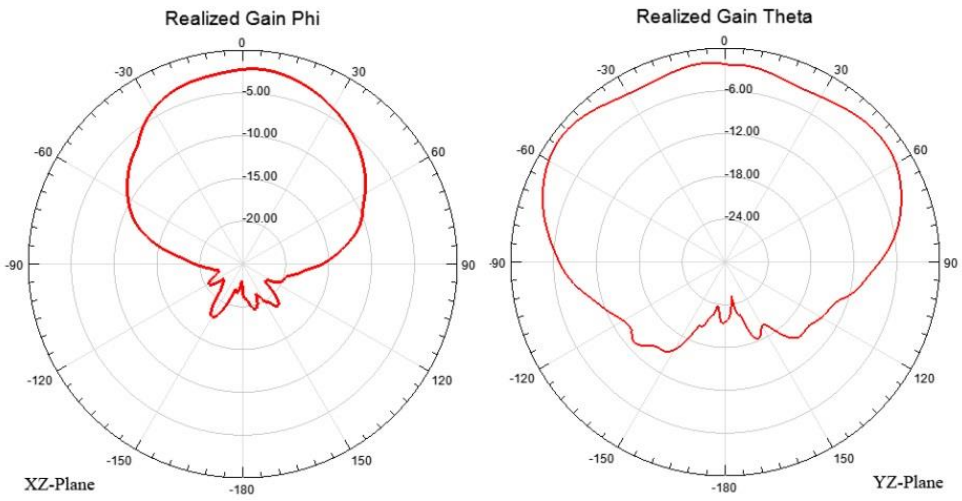

Figure 30. Wireless wearable module peak realized gain radiation pattern.

The calculated back-to-front ratio is now 40.149, consistent with Figure 29 where the power is concentrated in the front of the module. The directivity has increased from 3.6dB in free-space to 6.01dB as more power can be focused towards a given direction; however, the realized peak gain is -3.52dBi which reflects in a low antenna efficiency of 20.5% [26], which means that 79.5% of the antenna's accepted power is not being radiated. These results are the limiting case in which the wireless module is worn directly on the body; however, it will generally be worn on a belt or some sort of casing on top of clothing. Therefore, the next section analyses the wireless module at different distances from the body.

4.2.5 Parametric analysis

The limiting SAR and antenna detuning case has been already studied, and the result was satisfactory. However, the efficiency of the antenna was compromised as well

as the realized gain. HFSS has a feature called *optimetrics*, which allows to set-up a parametric analysis of a variable based on physical changes in the model. A parametric analysis was set-up to analyze the efficiency and realized gain of the wireless module at various distances from the body model. The efficiency results are shown in Figure 31.

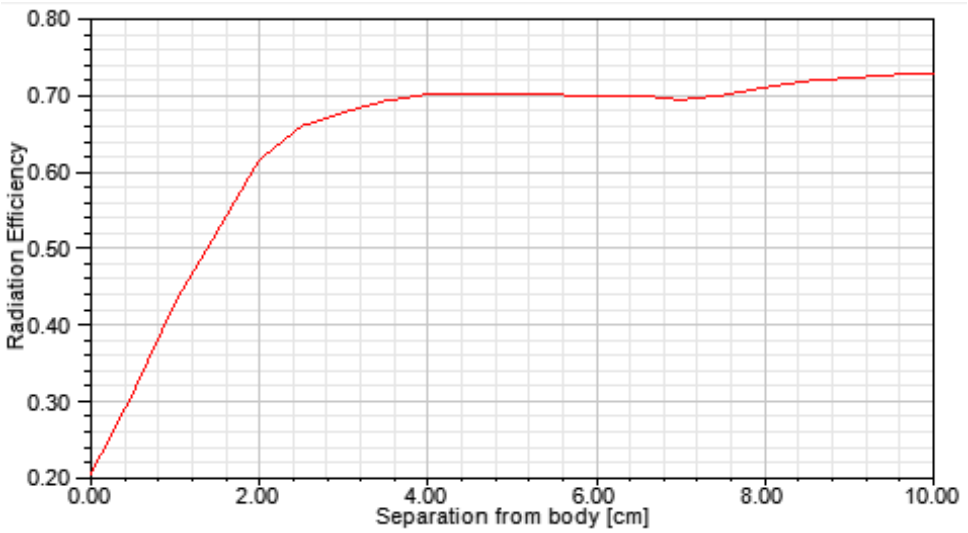

Figure 31. Radiation efficiency of wireless module at various distances from tissue.

The efficiency of the wireless module rapidly increases for small changes in the distance from the body. For 2cm away from the body, for example, an efficiency of more than 60% is observed. In the same way, a parametric analysis was conducted for the peak realized gain of the wireless module for various distances as seen in Figure 32.

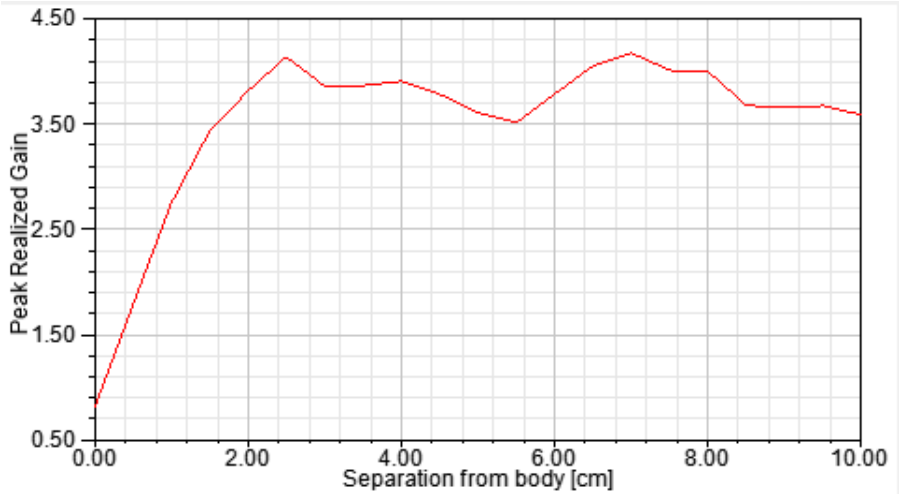

Figure 32. Peak realized gain of module at various distances from tissue.

As it was observed for the efficiency, the peak realized gain also improves rapidly at a small distance away from the body. At 1.5 cm from the body model, the efficiency is more than 3dBi. It is important to mention that as the distance between the body model and the wireless module increase, the relationship *phantom's height >> antenna* becomes less proper; however, for small distances such as 2cm, the relationship is assumed to remain appropriate. These results are promising in using inkjet printing not only for planar antennas but also 3D inkjet-printed antennas and modules.

CHAPTER 5

CONCLUSION

Inkjet-printing technology has been described as an innovative technique with the potential to revolutionize wireless electronics, especially applications that require low-cost, light-weight, biocompatible and/or eco-friendly designs. During the last years, inkjet-printing technology research has demonstrated the potential of this technology by focusing in antenna design and system-level-integration. Generally, system-level-integration used simplified designs that did not compare with the complexity achievable by traditional manufacturing techniques, such as commonly found wireless modules on FR-4. This thesis showed the design of a fully-integrated complex module on both FR-4 and paper substrate, and uncovered the challenges that require solutions in order to realize the potential of inkjet printing technology. Inkjet-printing technology must use reflowing in its manufacturing process, so that the assembly process can reduce the probability of short circuits, enable self-alignment of surface mount components, enable error-correction, and improve long-term reliability. Via holes must be implemented in the manufacturing process as well as a protective layer. Low-cost multi-material 3D inkjet-printing recently shown in research labs provides a solution of having a fully-integrated manufacturing process that would significantly reduce the price and complexity of current inkjet printing manufacturing. Novel applications of SWIM are presented in the area of wearable and implantable electronics, which are especially suited for 2D and 3D inkjet printing manufacturing.

REFERENCES

[1] Ian Akyildiz and Mehmet Can Vuran, *Wireless Sensor Networks*. Hoboken, NJ, USA: Wiley, 2010, pp. 1-35.

[2] N.P. Mahalik, Sensor networks and configuration : fundamentals, standards, platforms, and applications. Berlin, Germany: Springer, 2007, p. 1.

[3] Li Yang, Amin Rida, and Manos Tentzeris, *Design and Development of Radio Frequency Identification (RFID) and RFID-Enabled Sensors on Flexible Low Cost Substrates*, Amir Mortazawi, Ed. U.S.A.: Morgan & Claypool, 2009.

[4] Jong-In Ryu, Dongsu Kim, Jun Chul Kim, Hyeongdong Kim, and Jong Chul Park, "A System-on-Package Module by Fully Embedding Chip Components on Organic Substrate," in *Microwave Integrated Circuits Conference (EuMIC),* 2010, pp. 313 - 316.

[5] Koichiro Gomi, Masaaki Ishida, and Shigeru Hiura, "UWB Module with Antenna Using Organic Substrates," in *European Microwave Conference*, 2005 , p. 4.

[6] S. Lam et al., "Realization of a 27-MHz wireless transmitter using embedded passives on a thin organic substrate," in *Electronic Components and Technology Conference*, vol. 2, 2005, pp. 1704 - 1710.

[7] Dohyuk Ha et al, "3D Packaging Technique on Liquid Crystal Polymer (LCP) for Miniature Wireless Biomedical Sensor," in *2010 IEEE MTT-S International* , 2010 , pp. 612 - 615.

[8] Daniel Tobjörk and Ronald Österbacka, "Paper Electronics," *Advanced Materials*, vol. 23, no. 17, pp. 1935–1961, March 2011.

[9] Vasileios Lakafosis et al., "Progress Towards the First Wireless Sensor Networks Consisting of Inkjet-Printed, Paper-Based RFID-Enabled Sensor Tags," in *Proceedings of the IEEE*, 2010, pp. 1601 - 1609.

[10] N.P. Mahalik, Sensor networks and configuration : fundamentals, standards, platforms, and applications. Berlin: Springe, 2007, ch. 1, pp. 4-6.

[11] Audun Andersen. Design Note DN003. http://ti.com.

[12] Li Yang, Amin Rida, Rushi Vyas, and Manos M Tentzeris, "RFID Tag and RF Structures on a Paper Substrate Using Inkjet-Printing Technology," IEEE Transactions on Microwave Theory and Techniques, vol. 55, no. 12, pp. 2894 - 2901, 2007.

[13] Nithya R Subramanian. 0404 Balun Application Note ANN-2002. http://ti.com/.

[14] Dan McMahill. (2003) Microstrip Analysis/Synthesis Calculator. http://mcalc.sourceforge.net/.

[15] G.E. Jonsrud. Application Note AN040. http:/ti.com.

[16] Joyce Kwan, "Design of electronics for a high-resolution, multi-material, and modular 3D printer," M.A. Thesis, Massachusetts Institute of Technology (2013).

[17] A. Yakovlev, K. Sanghoek, A. Poon, "Implantable biomedical devices: Wireless powering and communication," *Communications Magazine, IEEE* , vol.50, no.4, pp.152-159, April 2012

[18] C. Cibin, P. Leuchtmann, M. Gimersky, R. Vahldieck, S. Moscibroda, "A flexible wearable antenna," Antennas and Propagation Society International Symposium, 2004. IEEE , vol.4, no., pp. 3589- 3592 Vol.4, 20-25 June 2004

[19] H.J. Visser, R.J.M. Vullers, "A miniature printed antenna with outer surface cable current suppression and low proximity effects," Antennas and Propagation (EUCAP), Proceedings of the 5th European Conference on , vol., no., pp.1837-1841, 11-15 April 2011

[20] S. Kim, Y. Ren, H. Lee, A. Rida, S. Nikolaou, M.M. Tentzeris, "Monopole Antenna With Inkjet-Printed EBG Array on Paper Substrate for Wearable Applications," Antennas and Wireless Propagation Letters, IEEE , vol.11, no., pp.663-666, 2012

[21] S. Bashir, M. Hosseini, R.M. Edwards, M.I. Khattak, L. Ma, "Bicep mounted low profile wearable antenna based on a non-uniform EBG ground plane - flexible EBG inverted-l (FEBGIL) antenna," Antennas and Propagation Conference, 2008. LAPC 2008. Loughborough , vol., no., pp.333-336, 17-18 March 2008

[22] P. Salonen, L. Sydanheimo, M. Keskilammi, M. Kivikoski, "A small planar inverted-F antenna for wearable applications," Wearable Computers, 1999. Digest of Papers. The Third International Symposium on , vol., no., pp.95-100, 1999

[23] X. Zhang, A. Zhao, "Enhanced-bandwidth PIFA Antenna with a Slot on Ground Plane," *PIERS Proceedings*, vol., no., pp.1268-1272, 2009

[24] A.S.Y. Poon, S. O'Driscoll, T.H. Meng, "Optimal Frequency for Wireless Power Transmission Into Dispersive Tissue," Antennas and Propagation, IEEE Transactions on , vol.58, no.5, pp.1739-1750, May 2010

[25] A. Yakovlev, D. Pivonka, T. Meng, A. Poon, "A mm-sized wirelessly powered and remotely controlled locomotive implantable device," Solid-State Circuits Conference Digest of Technical Papers (ISSCC), 2012 IEEE International , vol., no., pp.302-304, 19-23 Feb. 2012

[26] Frank Gustrau and Dirk Manteuffel, *EM Modeling of Antennas and RF Components for Wireless Communication Systems*.: Springer, 2006.

[27] Igor Egorov and Anders Dahlstrom, "Small-size broad-band printed antenna with parasitic element," Patent Application Publication 0050643, December 13, 2001.

[28] Steven R. Best, "The Significance of Ground-Plane Size and Antenna Location in Establishing the Performance of Ground-Plane-Dependent Antennas," *IEEE Antennas and Propagation Magazine*, vol. 52, no. 6, pp. 19 - 40 , 2010.

[29] M.-C. Huynh and W. Stutzma, "Ground plane effects on planar inverted-F antenna (PIFA) performance," *IEE Proceedings on Microwaves, Antennas and Propagation*, vol. 150, no. 4, pp. 209 - 213, 2003.

[30] Barry Levy, David Wegman, Sherry Baron, and Rosemary Sokas, *Occupational and Environmental Health: Recognizing and Preventing Disease and Injury*. New York, United States: Oxford University Pres, 2011.

[31] Danielle Dellorto, "WHO: Cell phone use can increase possible cancer risk," *CNN*, May 2011.

[32] Federal Communications Commission (FCC), Evaluating Compliance with FCC Guidelines for Human Exposure to Radiofrequency Electromagnetic Fields, 2001, SUPPLEMENT C (Edition 01-01) to OET BULLETIN 65 (Edition 97-01).

[33] Soo Liam Ooi, UHF Handset Monopole Antenna Designed for SAR compliance, Center for Wireless Access Motorola Labs.

[34] Anis Koubâa, Mario Alves, and Eduardo Tovar , "IEEE 802.15.4: a Federating Communication Protocol for Time-Sensitive Wireless Sensor Networks," in *Sensor Networks and Configurations: Fundamentals, Techniques, Platforms, and Experiments*. Germany: Springer-Verlag, 2006.

[35] Nello Carrara. (2010) Dielectric Properties of Body Tissues in the frequency range 10 Hz - 100 GHz. [Online]. "http://niremf.ifac.cnr.it/tissprop/"